Journal of Structural Geology 75 (2015) 49–59

Contents lists available at ScienceDirect

Journal of Structural Geology

journal homepage: www.elsevier.com/locate/jsg

Spatial arrangement of décollements as a control on the development of thrust faults

Lian Feng [a, *], Mervin J. Bartholomew [a], Eunseo Choi [b]

[a] Department of Earth Sciences, The University of Memphis, Memphis, TN 38152, USA
[b] Center for Earthquake Research and Information, The University of Memphis, Memphis, TN 38152, USA

ARTICLE INFO

Article history:
Received 12 August 2014
Received in revised form
24 February 2015
Accepted 5 March 2015
Available online 21 March 2015

Keywords:
Numerical modeling
Décollement
Thrust fault
Ramp-flat
Imbricate
Duplex

ABSTRACT

We used two-dimensional finite element models to explore different configurations of weak layers in undeformed sedimentary sequences to investigate the occurrence of three characteristic types of thrust configurations: ramp-flat; imbricate; and duplex. In our models, we embedded two low-friction weak layers with a finite spatial extent in a sequence of stronger rock. These two weak layers were initially horizontal, were separated vertically by 1 km, and were arranged in three different relative positions to each other. When the models were deformed and these weak layers developed into décollements, they interacted to produce one of the three types of thrust faults as a function of their initial configurations. When the tips of weak layers were separated by a large gap (>10 km), only the lower-level décollement became active, producing imbricate thrusts. When the two weak layers overlapped for a large distance (>10 km), they simultaneously became active décollements, producing duplexes in the overlapped zone. When the gap or overlap was small (<5 km), the two weak layers also simultaneously became active décollements but their tips linked up to form a ramp-flat geometry. These results suggest that thrust geometry is highly sensitive to the initial arrangement of décollements.

1. Introduction

This study grew out of regional mapping (e.g. Bartholomew and Lowery, 1979; Bartholomew et al., 1981; Schultz, 1986, 1988; Bartholomew, 1987; Bartholomew and Brown, 1992; Schultz and Bartholomew, 2009, 2010) and outcrop-scale studies (e.g. Schultz, 1979; Bartholomew et al., 1980, 1982; Gray, 1981; House and Gray, 1982; Simon and Gray, 1982; Schultz, 1986; Onasch and Dunne, 1993; Couzens et al., 1993; Bartholomew et al., 1994; Whitaker and Bartholomew, 1999; Spraggins and Dunne, 2002; Bartholomew and Whitaker, 2010) in the Roanoke recess of the Appalachian fold-and-thrust belt in an effort to understand why some thin, weak layers developed into intensely deformed zones whereas, elsewhere the weak layers were significantly less strained. In this paper, we used the terms “weak” or “incompetent” to describe rocks that have low frictional strength and cohesion relative to “strong” or “competent” rocks. We reserved the term “décollement” for a gliding zone of accumulated high shear strain.

Early modeling by Apperson and Bartholomew (1992) examined the relationship between the intensity of deformation of a thin weak unit, beneath a flat between two ramps, and the length of that flat. Their preliminary results suggested that:

1. ramps functioned independently for a flat-length of 10 km;
2. ramps merged into a single ramp for a flat-length of 1 km;
3. but for a flat-length of 5 km, the thin weak layer beneath the flat extended for the length of the flat as a highly strained zone.

The last result was consistent with extensive duplexing in a weak zone, observed in outcrops in Middle-Upper Ordovician strata, below a flat in the above-cited work in the recess (e.g. Gray, 1981; Simon and Gray, 1982; Couzens and Dunne, 1994). Additionally, Smart et al. (1997) showed that, farther north in the central Appalachians, 75% of the shortening of the roof sequence, above a weak zone in Middle-Upper Ordovician strata, was accommodated by micro- and meso-scale structures during duplex emplacement. Similarly, the weak zone in Silurian salt, still farther north in Pennsylvania, allowed decoupling of the roof sequence during emplacement of the Cambrian-Ordovician duplexes (Gwinn, 1964, 1970; Nickelsen, 1988).

* Corresponding author. Tel.: +1 901 678 1421.
E-mail addresses: lfeng@memphis.edu (L. Feng), jbrthlm1@memphis.edu (M.J. Bartholomew), echoi2@memphis.edu (E. Choi).

http://dx.doi.org/10.1016/j.jsg.2015.03.002
0191-8141/

We also noted that many fold-and-thrust belts have more than one weak zone above the basal décollement, and they have developed into décollements at different depths (e.g. Price and Fermor, 1985; Williams and Dixon, 1985; Wilson and Schumaker, 1992; Belotti et al., 1995). Weak zones may extend across the entire fold-and-thrust belt but are more likely to be less continuous due to syn-orogenic changes in depositional environments. However, most previous studies, that were concerned about deformations in a thrust system, considered only one weak layer or alternating continuous weak layers extending across the entire width of a fold-and-thrust belt (e.g. Buiter et al., 2006; Selzer et al., 2007; Konstantinovskaya and Malavieille, 2011; Simpson, 2011; Ruh et al., 2012). These models provided valuable insights on development of an entire thrust wedge but such "layer-cake" models clearly precluded investigation on the evolution of a thrust system with multiple discontinuous décollements.

The presence of multiple discontinuous décollements in a fold-and-thrust belt and their potential importance for local thrust geometry led us to question how gaps and overlaps of weak zones determine thrust geometry. Three major types of thrust geometries found in fold-and-thrust belts are:

- a ramp-flat structure (Fig. 1a), a thrust with a stair-step trajectory (Rich, 1934);
- an imbricate thrust system (Fig. 1b) that consists of sequentially formed subparallel thrust faults that develop from a common basal décollement (Boyer and Elliott, 1982);
- a duplex (Fig. 1c) that forms when splays asymptotically curve upward and link with a higher-level décollement rather than terminate up-section (Boyer and Elliott, 1982).

A fold-and-thrust belt typically contains complex thrust systems that exhibit all three geometries and this observation forms the basis for our hypothesis that the type of thrust geometry is determined by the local configuration of discontinuous décollements. Appearance of all three geometries in fold-and-thrust belts was documented in the Appalachians (e.g. Rich, 1934; Rodger, 1950; Mitra, 1986; Bartholomew, 1987; Evans, 1989), the Canadian Rockies (e.g. Dahlstrom, 1970; Price, 1981), the Alps (e.g. Ramsay, 1981; Boyer and Elliott, 1982) and Taiwan (e.g. Suppe, 1980; Davis et al., 1983). Here we choose the central Appalachians to illustrate how all three may be found in transects that change westward across the fold-and-thrust belt:

- from where the imbricated, far-travelled (~50 km) Blue Ridge and North Mountain sheets overlie a duplicated section of lower-to-middle Paleozoic strata (e.g. Evans, 1989, 2010);
- to the extensive blind duplex (used by Boyer and Elliott, 1982) of thick, strong, Cambrian-Ordovician carbonates that ends with the Wills Mountain structure (e.g. Evans, 1989; Wilson, 1989; Wilson and Shumaker, 1992; Evans, 2010);
- where, imbricates then cut across thin, but strong, near-vertical Silurian quartzite which forms the structural front of the fold-and-thrust belt (e.g. Evans, 1989, 2010);
- to the foreland where a few ramp-flat structures cut upward from middle Ordovician to Devonian strata (e.g. Evans, 1989, 2010) and megascopic and microscopic structures account for 10–15% shortening (Engelder and Engelder, 1977; Dean et al., 1988; Smart et al., 1997; Spraggins and Dunne, 2002; Evans, 2010).

Physical and numerical models have long been used to study deformation in fold-and-thrust belts (e.g. Erickson, 1995; Smart et al., 1999; Smart and Couzens-Schultz, 2001; Buiter et al., 2006; Selzer et al., 2007; Stockmal et al., 2007; Simpson, 2009; Konstantinovskaya and Malavieille, 2011; Ruh et al., 2012). Some modeling studies particularly addressed structural evolution of a fold-and-thrust belt with single *versus* multiple and viscous *versus* frictional décollements. Regardless of technical differences among modeling methods, the following have been commonly found in the results: (1) Formation of in-sequence forelandward-propagated thrusts accommodated most strain whether the rheology of décollement was frictional or viscous (Buiter et al., 2006; Selzer et al., 2007; Stockmal et al., 2007; Simpson, 2009; Konstantinovskaya and Malavieille, 2011); (2) backward-verging thrusts formed in thrust belts over a viscous décollement (Simpson, 2009; Ruh et al., 2012); (3) more than one décollement produced more complex structures like fault-bend folds, duplexes,

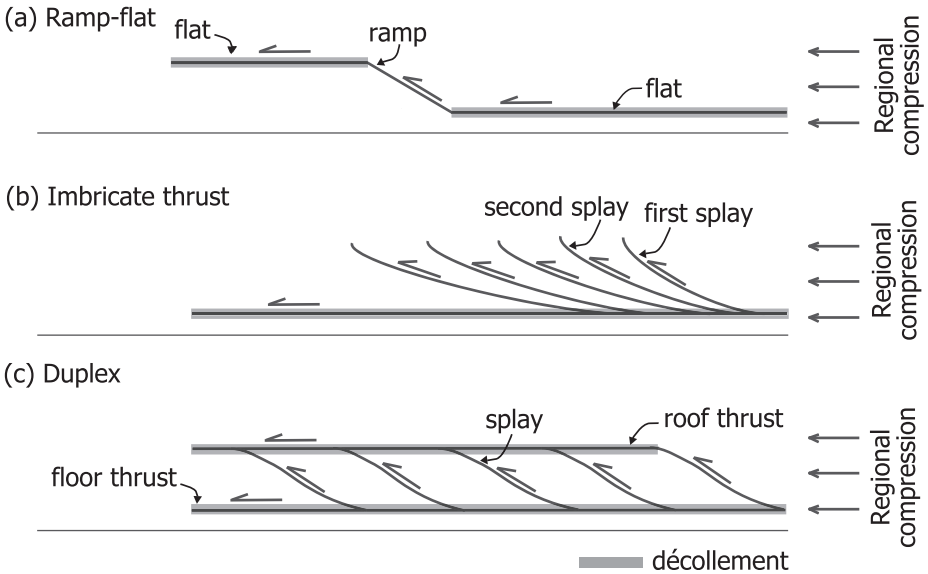

Fig. 1. Diagrams depicting three types of thrusts. (a) Ramp-flat geometry modified from Rich (1934). (b) Imbricate thrusts modified from Boyer and Elliott (1982). (c) Duplexes. Shaded layers demarcate décollement levels. Black lines and arrows indicate faults and their sense of motion.

fault propagation folds, tectonic underplating and antiformal stacking (Stockmal et al., 2007; Konstantinovskaya and Malavieille, 2011; Ruh et al., 2012).

Multiple discontinuous décollements in a fold-and-thrust belt and their potential importance for thrust geometry motivated our investigation on the correspondence between thrust geometry and weak layers in an undeformed rock sequence. Through systematic control of the weak layer configuration in the numerical models, we offer insights into which initial configurations of décollements are responsible for the relative abundance of ramp-flats, imbricate fans and duplexes in thrust systems.

2. Numerical method

2.1. Numerical solver

We used DynEarthSol2D (Choi et al., 2013), a two-dimensional, explicit, unstructured finite-element solver. Being open source, it is available at http://bitbucket.org/tan2/dynearthsol2. DynEarthSol2D is built upon the same set of governing equations and solution procedures as for FLAC (Cundall and Board, 1988; Poliakov et al., 1994; Lavier et al., 2000). The most useful new feature of DynEarthSol2D is the flexibility in meshing that is enabled by the use of unstructured grids. Unlike its predecessors, DynEarthSol2D can easily refine a mesh around a fine-scale structure. It also can dynamically refine and coarsen the initial mesh as strain localizes in fault zones (Choi et al., 2013). These features render this code suitable for modeling deformations that involve formation and evolution of multiple faults. All models presented in this paper were run on a cluster at the High Performance Computational Center of the University of Memphis. Each compute node of the cluster has an AMD Dual Opteron 8356 (Shanghai) 2.5 GHz Quad Core and 32 GB (16×2 GB) DDR2-667 RAM. Each model was run on a single core and took about 96 h to generate 10 km of shortening in our model setting.

2.2. Model geometry

For the sake of keeping models simple, yet geologically relevant, we imposed the following constraints, which are based on known characteristics of fold-and-thrust belts:

1. The belts are thin-skinned, i.e., thrusts are entirely confined to sedimentary rocks above the basement complex.
2. The model configuration is consistent with a layered sedimentary sequence that was deposited prior to horizontal shortening.
3. The presence of multiple weak layers within the rock sequence is common (Rich, 1934; Mitra, 1986; Bartholomew, 1987; Evans, 1989).
4. Perturbations such as fault shape, stratigraphy, pore fluid pressure, folding, and surface slope are not necessary for development of thrust faults (Panian and Wiltschko, 2004).

We constrained mechanical stratigraphy in our models based on the simplified Paleozoic sedimentary sequence from the northern end of the southern Appalachian fold-and-thrust belt (Bartholomew, 1987). Here, a regional basal detachment is in the Cambrian Rome Formation and is overlain sequentially by: 1) 1300 m of relatively strong Cambro-Ordovician shelf carbonates; 2) 400 m of middle to upper Ordovician calcareous mudstones/siltstones; 3) 400 m of extremely strong Silurian quartz arenites; 4) 1100 m of Devonian mudstones/siltstones and interlayered sandstones; 5) >1500 m of Mississippian sandstone-dominated clastic rocks. Thus, these lower Paleozoic rocks are divisible into three competent lithotectonic units that are separated by Ordovician and Devonian incompetent units (mudstones/siltstones) and the spatial extent of these two incompetent units do not entirely overlap each other (Harris and Milici, 1977; Bartholomew, 1987; Evans, 1989).

Models begin with a rectangular domain comprised of a static base with a deformable overlying layered sequence (Fig. 2). The base, corresponding to marker layer 3 in Fig. 2, is a 2 km-thick layer of competent rock and is fixed both horizontally and vertically along the bottom as well as along the right- and left-hand boundaries. Above the base is a 6 km-thick layer of competent rock in which two different colors are used to show an alternating sequence of marker layers as a proxy for bedding in every model. Two 500 m-thick weak layers are at depths of ~4.5 and ~6 km, respectively. The domain is discretized into triangular elements with a ~180 m long edge on average but smaller elements are created when new nodes are inserted into shear bands during remeshing (Choi et al., 2013). As a result, elements within a shear band have an average edge length of 68 m.

Both the vertical and horizontal spacing between the weak layers are adjustable. However, our preliminary tests showed that the influence of vertical spacing on thrust geometry is not as significant as the horizontal spacing (compare Fig. A1b with Fig. A1a). Therefore, for the models presented here, the vertical spacing between the weak layers is held constant at 1 km. The horizontal spacing (ΔL) is defined as $L_1 - L_2$, where L_1 is the location of the right end of the shallower incompetent layer, measured from the left boundary of the domain, and L_2 is the location of the left end of the deeper incompetent layer. With these definitions, a positive value of ΔL corresponds to overlapping incompetent layers whereas a negative value corresponds to a gap.

2.3. Material model

Rocks start to experience permanent deformation when differential stress exceeds a certain yield condition. Faults or fault zones can be considered as one of the localized forms of permanent deformation. Strength of brittle materials like rock, by definition of brittleness (e.g. pp. 80, Jaeger and Cook, 1976), degrades with accumulating permanent strain. To represent such behaviors of rocks in our continuum models, we employ the non-associated Mohr-Coulomb plasticity model with strain weakening. This constitutive model allows for localization of plastic strain in the form of shear bands that behave like faults (e.g. Buck, 1988; Lavier et al., 2000; Ellis et al., 2004; Ruh et al., 2012). Although formation of shear bands can occur without strain weakening (e.g. Vardoulakis, 1980), we enforced strain weakening to unconditionally induce the formation of shear bands. In our formulation of strain weakening, plastic parameters such as friction angle and cohesion are linearly reduced as plastic strain increases (e.g. Lavier et al., 2000; Ellis et al., 2004; Ruh et al., 2012).

The mechanical lithology in our models is categorized as incompetent and competent layers only, and identical material properties are assigned to each type. Therefore, Cambro-Ordovician shelf carbonates and Silurian quartz-arenites are classified as competent layers, likewise, Devonian mudstones/siltstones and upper Ordovician calcareous mudstones/siltstones are treated as the same type of incompetent rock.

Our model sensitivity tests suggested that deformation behaviors are not significantly affected by geologically reasonable variations in elastic moduli and density (compare Figs. A1c and A1d with Fig. A1a). Thus we used a constant shear modulus and bulk modulus for all lithologies in the models: 3 GPa and 5 GPa, respectively.

For plasticity, the cohesion and friction angle of competent layers are subjected to strain weakening and decrease linearly from $C_0 = 40$ MPa and $\varphi_0 = 30^\circ$ to their minima, 10% of C_0 and 50% of φ_0,

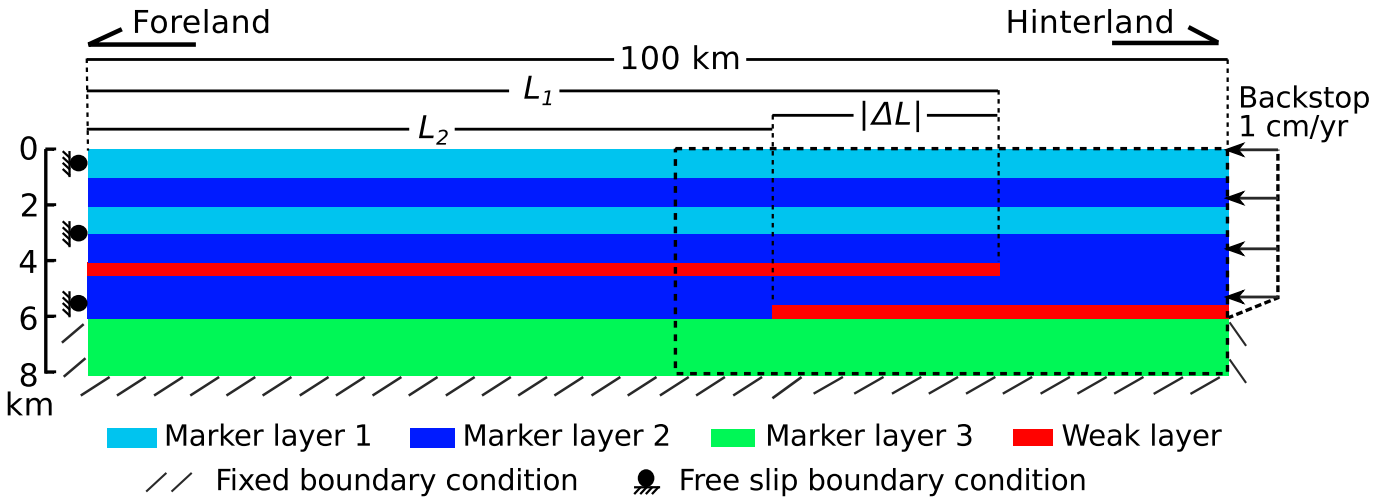

Fig. 2. Model setup and boundary conditions. The dotted box outlines the part of the model domain shown in subsequent figures. See text for further explanation.

respectively, with increasing plastic strain up to 10. Although a plastic strain measure of 10 seems high, it is not extreme for shear bands that are dynamically refined as in our models. The nominal value of plastic strain is equivalent to the critical fault offset of ~2 km for the ~200 m-wide shear bands (element size of 68 m × 3 elements composing a shear band) of our models according to the formulation proposed by Lavier et al. (2000). They showed that defining the weakening rate in terms of the critical offset rather than plastic strain effectively eliminated element size-dependent behaviors for shear bands. The critical offset of 2 km used in this study is within the range of values adopted in other studies (e.g. Smart et al., 1999; Lavier et al., 2000; Stockmal et al., 2007). Cohesion and friction angles employed for competent layers in our models are within the general range reported in experimental data (e.g. Zoback, 2007). Décollements in shale are often represented by frictionally weak layers with a much smaller Mohr-Coulomb failure criterion than the overlying material. So, the friction angle is fixed at 1° and cohesion is zero for weak layers in this study, which are comparable to those values used in previously similar work (Selzer et al., 2007; Stockmal et al., 2007; Ruh et al., 2012). Some numerical modeling experiments showed that models with lower cohesion for thrust systems are more comparable to analogue models (e.g. Ellis et al., 2004). Thus cohesion values for incompetent layers in frictional models are often smaller than the suggested values for shale layers in physical experiments (e.g. Colmenares and Zoback, 2002). A complete list of material properties used in this study is given in Table 1.

2.4. Initial and boundary conditions

A gravitational body force is always applied and a lithostatic stress state is assumed as the initial condition in our models. Along the right hand boundary above the base, both a constant horizontal velocity ($v_x = -1$ cm/yr) and a zero vertical velocity ($v_z = 0$) are applied. The horizontal velocity is linearly reduced to zero from the top to the bottom of the right end of the lower weak layer. The left boundary above the base has a free-slip condition (Fig. 2). The velocity boundary condition applies an incrementally increasing displacement boundary condition. Therefore, time and velocity do not have meaning for our models individually, but the product of them, i.e., displacement, does. Syndeformational exhumation results in sediments deposited toward the foreland during and after the orogenic process (e.g. Dahlen and Barr, 1989), and many modeling studies showed that surface process plays an important role on deformation in the foreland fold-and-thrust belts (e.g. Bonnet et al., 2007; Malavieille, 2010). In this study, a diffusion-like topographic smoothing model (Culling, 1960) is applied to the top boundary. Surface processes approximated by this model have been taken into account in previous studies on thrust systems such as Selzer et al. (2007) and Ruh et al. (2012). Culling's model assumes that the time rate of change of topography is proportional to the surface curvature, yielding the following diffusion equation:

$$\frac{\partial h}{\partial t} = \kappa \nabla^2 h$$

where h is the surface topography and κ is the transport coefficient. The value of κ is 3.15 m^2/yr in all of our models, which is in the range of 0.05–5 m^2/yr (Allen, 1997; Kühni and Pfiffner, 2001).

3. Results

We ran 9 models where ΔL varied from − 20 to 20 km at 5-km increments. We displayed model results with up to 10 km of backstop displacement, where the thrusting style is unambiguously

Table 1
Material properties used for mechanical stratigraphy.

Parameter	Description	Weak layer	Strong layer (marker layer 1–3)
G	Shear Modulus (GPa)	3	3
K	Bulk Modulus (GPa)	5	5
C_0	Initial Cohesion (MPa)	0	40
C_1	Reduced Cohesion (MPa)	0	4
φ_0	Initial Friction angle (°)	1	30
φ_1	Reduced Friction angle (°)	1	15
ε_p	Critical plastic strain	0.1	10
Ψ	Dilation angle (°)	0	0
ρ	Density (kg/m^3)	2500	2600

identified. We describe three models in detail that each clearly reproduced one of the three thrusting styles.

3.1. Model with a large gap ($\Delta L = -20$ km)

This model developed an imbricate style of thrusting (Fig. 3). The lower-level weak layer underwent simple shear, and developed into a décollement. Two localized plastic strain bands initiated from the basal décollement at 12 km away from the backstop becoming conjugate shear bands branching upward. They are interpreted to represent an imbricate splay and its associated back-thrust (Fig. 3a). These thrusts propagated upward at an ~40° dip into the overlying strong rock. An uplifted hanging wall block between the conjugate thrusts defined a pop-up structure (Fig. 3b). The first imbricate splay remained active and accumulated more strain than the first back-thrust, which became inactive as a second back-thrust initiated at the juncture of the lower flat and the first splay (Fig. 3c). After about 6 km of the backstop displacement, the basal décollement was reactivated in front of the first imbricate splay and the second imbricate splay formed at the termination of the basal décollement (Fig. 3d). Gradually, plastic deformation below the second back-thrust became diffuse and its formation gave way to development of second splay in the foreland direction (Fig. 3e). With continued shortening, a new backward plastic strain band appeared at the juncture of the lower flat and the second splay (Fig. 3f). At no point during this simulated deformation history did the upper weak layer activate and become part of the thrust system.

3.2. Model with zero gap/overlap ($\Delta L = 0$ km)

This model developed a ramp-flat geometry (Fig. 4). Both weak layers started to function as décollements from the earliest stage.

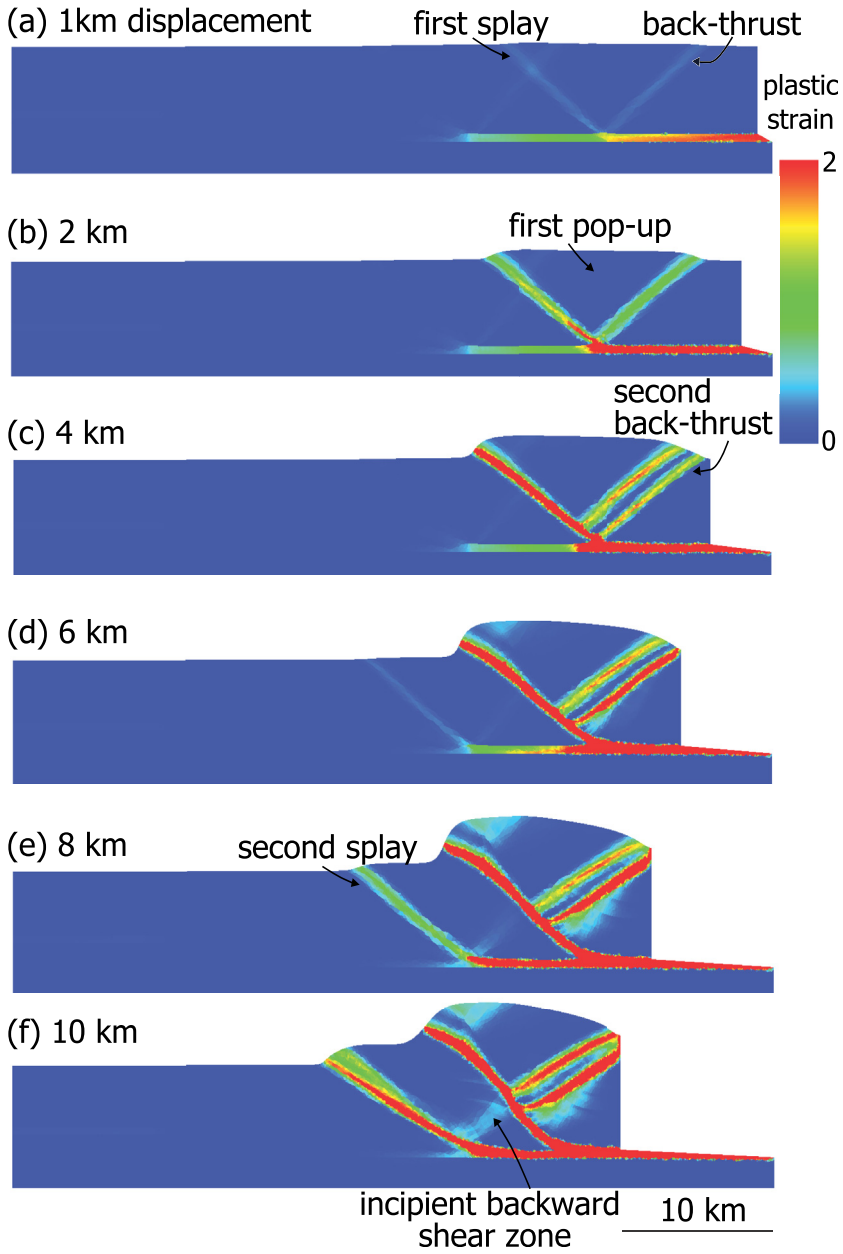

Fig. 3. Snapshots of the model with $\Delta L = -20$ km. (a) to (j) corresponds to 1–10 km of the backstop displacement.

Ramps initiated from the adjacent tips of the two décollements, but only the one ramp developed a conjugate back-thrust that remained active (Fig. 4a). A flat-ramp-flat structure formed when the active ramp linked the tips of the two décollements at a 27° dip (Fig. 4b). The primary ramp continued to grow, cutting up-section, and subsequently producing an asymmetric pop-up together with an active back-thrust dipping at ~47° (Fig. 4c). Then, a new set of conjugate thrusts initiated from the upper décollement, 15 km to the left of the first ramp. The second thrust dipped ~40° and its back-thrust ~42°, creating the symmetric second pop-up structure (Fig. 4d). A series of sub-parallel, backward shear bands appeared as material moved over the lower flat-ramp hinge. Given the small amount of strain observed in sequential backward shear bands, they may reflect distributed strain in the hinge of fault-bend folds rather than formation of well-developed back-thrusts (Fig. 4e). The conjugate thrusts, which formed the second pop-up, accommodated most of the subsequent shortening (Fig. 4f).

3.3. Model with a large overlap ($\Delta L = 20$ km)

The duplex style emerged in this model (Fig. 5). As in the previous model, both weak layers quickly became décollements (Fig. 5a). After 2 km of backstop displacement, multiple sets of conjugate thrusts formed almost simultaneously in the cross-sectional area between the two overlapping décollements (Fig. 5b). Subsequently, the upper décollement started to function as a roof thrust and the lower décollement as a floor thrust. Two active splays between the roof and floor thrusts linked them together to complete a duplex (Fig. 5c). Soon afterwards, the roof thrust merged with the first back-thrust, producing a major backward roof thrust (Fig. 5d). As the roof thrust reversed its sense of motion, the original duplex became a passive-roof duplex (Fig. 5e). Material pushed in by the backstop propagated forelandward beneath the roof thrust. At about 10 km of backstop displacement, the roof back-thrust was still the dominant secondary fault in the

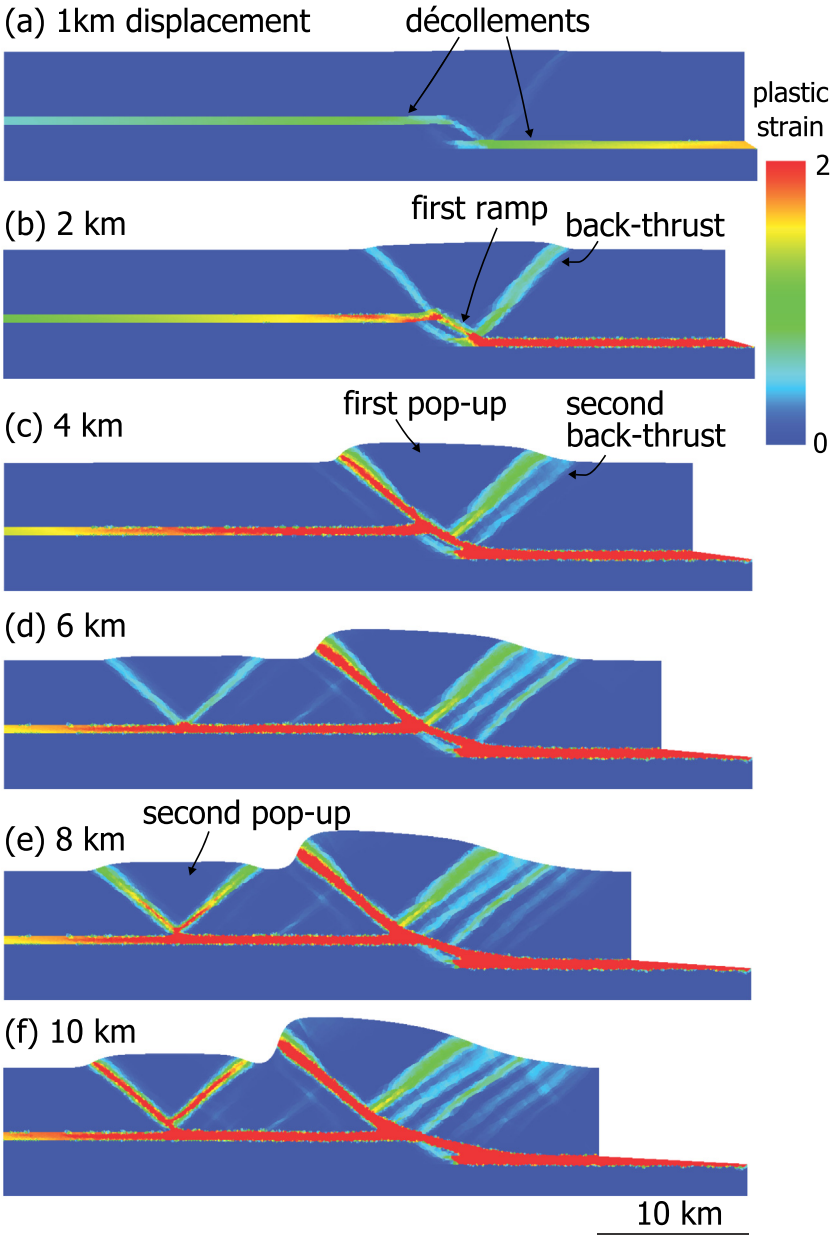

Fig. 4. Same as Fig. 3 but $\Delta L = 0$ km.

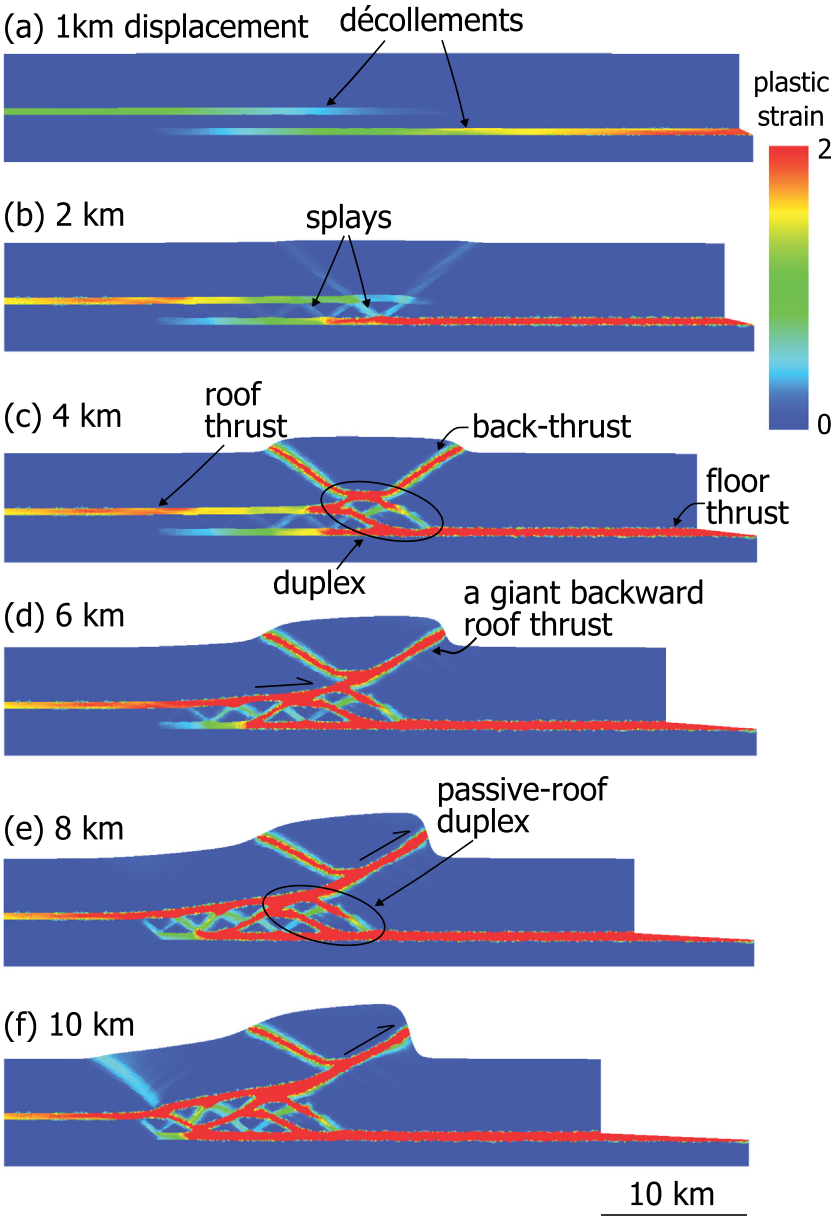

Fig. 5. Same as Fig. 3 but $\Delta L = 20$ km.

deforming sequence, while a new hinterlandward shear band developed to accommodate a portion of the total shortening (Fig. 5f).

4. Discussion

Based on the results from our 9 models and some previous studies (e.g. Buiter et al., 2006; Selzer et al., 2007; Stockmal et al., 2007; Konstantinovskaya and Malavieille, 2011; Simpson, 2011; Ruh et al., 2012), we discuss the correspondence between the types of thrust geometry and the initial configurations of weak layers.

Imbricate splays and a series of back-thrusts developed in models with a large ($\Delta L \leq -15$ km) gap between the two weak layers (Fig. 6a,b). The model with a 10 km gap ($\Delta L = -10$ km) generated a thrust geometry with one imbricate splay (Fig. 6c). In these models, no failure occurred along the distal upper weak layer until the end of simulation and it did not become part of the thrust system. Thus, they behaved just like a thrust wedge overlying a single isolated décollement (e.g. Buiter et al., 2006; Selzer et al., 2007; Stockmal et al., 2007; Simpson, 2011; Ruh et al., 2012). Natural imbricate thrusts are common at various scales in fold-and-thrust belts of the world, e.g., the Canadian Rocky Mountains (Dahlstrom, 1970, Fig. 3), the Valley and Ridge Province in the southern Appalachians (Harris and Milici, 1977), the Wyoming overthrust (Dixon, 1982, Fig. 6), and the Taconic allochthons of the western New England (Stanley and Ratcliffe, 1985, Pl. 2).

When the upper weak layer was actively involved, interaction between the two weak layers changed with changes in the overlap/gap geometry. In models with a small or zero gap, i.e., with $\Delta L = -5$ km (Fig. 6d) or with 0 km (Fig. 6e), the ramp-flat style appeared. In these models, the two weak layers accumulated high strain simultaneously first, and then a ramp developed across the strong layers between them. Although a ramp-flat geometry

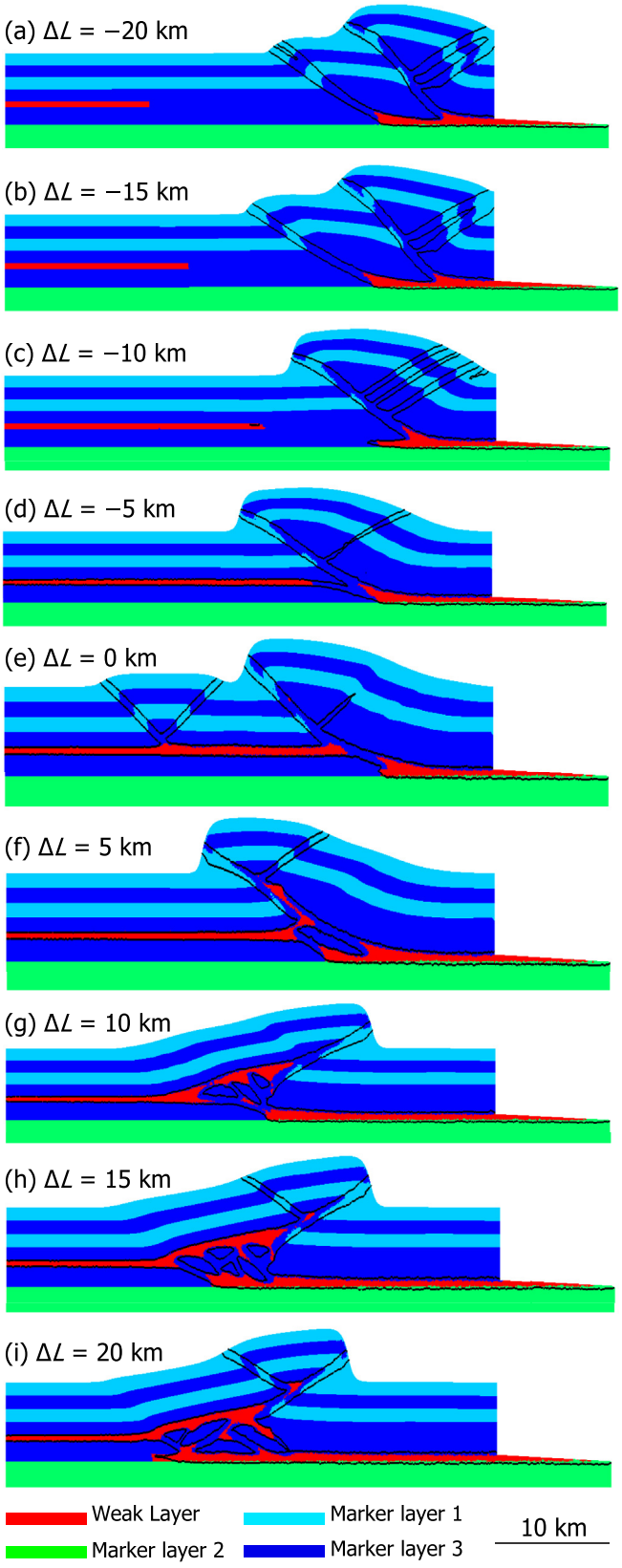

Fig. 6. Snapshots of all models at 10 km backstop displacement, arranged vertically from the greatest gap ($\Delta L = -20$ km) at the top to the greatest overlap ($\Delta L = 20$ km) at the bottom. Solid black lines are contours of plastic strain of 1.0.

initiated in the model of $\Delta L = -5$ km (Fig. 6d), the ramp was not optimally oriented. As a result, the initial ramp was eventually abandoned as a new thrust ramp with a greater dip appeared. In contrast, the model with $\Delta L = 0$ km (Fig. 6e) produced a ramp with a greater initial dip and subsequently the ramp induced a thrust that propagated forelandward to the surface. The Pine Mountain thrust/Powell Valley anticline (Rich, 1934, Figs. 3 and 4; Mitra, 1988) and the Sequatchie Anticline (Rodger, 1950, Fig. 3; Wojtal, 1992) in the southern Appalachians are geometrically similar to our modeled ramp-flat thrust.

Duplexes formed when décollements overlapped. In the model with a small overlap ($\Delta L = 5$ km), a regular duplex developed (Fig. 6f). The décollement configurations and the final thrust geometry of our model are comparable to natural duplexes at various scales observed in fold-and-thrust belts. For example, three-tiered duplexes underneath the Sandy Hollow thrust in the Cordilleran fold-and-thrust belt of southwest Montana exhibit a regular duplex geometry in the 27 m-thick limestone of the Kootenai Formation on the eastern limb of Sandy Hollow anticline (Sears et al., 1989, Fig. 6). In the Sandy Hollow Duplex, each duplex package consists of one competent 1–3 m-thick packstone/wackstone unit, one shale unit of the same thickness and another inferred décollement, which separates the duplex and a thick undeformed basal unit. Another good example is the Lower Carbonate duplex, which extends beneath the Blue Ridge and North Mountain thrust in the central Appalachians of northern Virginia (Evans, 1989, Fig. 10).

In models with a large overlap, i.e., $\Delta L = 10$ km (Fig. 6g), 15 km (Fig. 6h) and 20 km (Fig. 6i), a duplex with multiple horses and a passive-roof thrust formed. This complex thrust geometry was also observed in some previous studies where multiple weak layers overlapped completely (Konstantinovskaya and Malavieille, 2011; Ruh et al., 2012; Stockmal et al., 2007). In our models, a passive-roof duplex formed as the flat portion of the roof thrust merged with a major back-thrust. This roof back-thrust had the cover response to duplex emplacement that was observed in other models (e.g. Smart et al., 1999; Smart and Couzens-Schultz, 2001). The Wills Mountain duplex in the central Appalachian fold-and-thrust belt of central-east West Virginia is an exemplary passive-roof duplex. Its floor thrust (the incompetent Lower Cambrian Waynesboro Formation) and the roof thrust (the incompetent Middle-Upper Ordovician Martinsburg Formation) overlapped for several miles underneath the Wills Mountain Anticline (Kulander and Dean, 1986, section 2 of Fig. 6). Our simulated thrust (Fig. 6h,i) may represent deformation of this type of geometry.

Décollement zones that consist of viscous salt layers are also found in nature, and these salt layers have been modeled as viscously weak layers in some models (e.g. Ellis et al., 2004; Ruh et al., 2012). Although we assumed décollements are frictionally weak, our models that produced imbricate thrusts showed similar behaviors with a thrust system overlying a low-viscosity basal layer (see Fig. 11 of Ellis et al., 2004). Our model results indicated that the weakness of décollements relative to the surrounding rock is critical for determining thrust geometry. This weakness promoted forelandward propagation of a thrust system, thereby boosting the interaction of two décollements. Our conclusions on sensitivity of thrust geometry to initial configuration of weak layers would hold regardless of décollement rheology as long as décollements are sufficiently weak. This conditional indifference to rheology is also supported by field observations for décollements, e.g., in Wills Mountain duplex in the Appalachian Plateau of West Virginia, Smart et al. (1997) found that an Ordovician shale-dominated formation was sufficiently weak to act in a manner similar to that of a salt-dominated roof décollement.

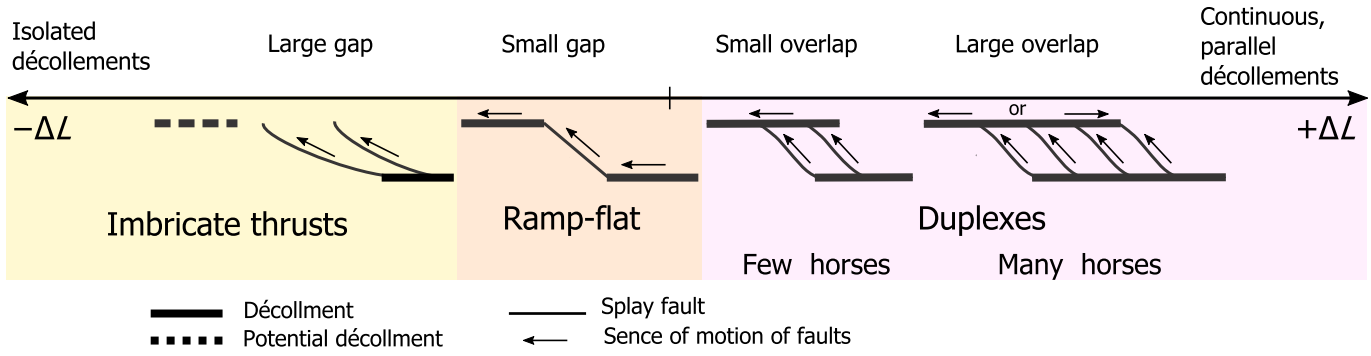

Fig. 7. Diagram showing the correspondence between thrust geometry and initial configurations of décollements.

5. Conclusions

Our finite element models showed that foreland thrust systems evolve differently based on changes in the initial configurations of weak layers. By changing the relative position of the tips of two horizontal weak layers at different depths, we obtained a full spectrum of thrust-system geometries from imbricate thrusts to ramp-flat thrusts to duplexes (Fig. 7). When two weak layers:

1) are separated by a large gap ($\Delta L \leq -15$ km), imbricate thrusts develop;
2) are separated by a small ($\Delta L = -5$ km) to zero ($\Delta L = 0$ km) gap, a ramp-flat thrust initiates
3) overlap by a small ($\Delta L = 5$ km) distance, a regular duplex forms;
4) overlap by a large distance ($\Delta L \geq 10$ km), a passive-roof duplex with many horses occurs.

Acknowledgements

L. Feng was supported by the Department of Earth Sciences and the Center for Earthquake Research and Information at the University of Memphis (UofM). The authors appreciate the generous use of the High Performance Computing Center of the UofM. R. T. Cox and R. B. Van Arsdale reviewed earlier versions of this manuscript. This paper greatly benefited from the comments of Kevin Smart, William Dunne, and an anonymous reviewer.

Appendix A

We presented results from extra models that showed relatively low sensitivity of thrust geometry to three model parameters: 1) the vertical separation of weak layers, 2) elastic moduli (G and K), and 3) density (ρ). Fig. A1 showed snapshots after 10 km of backstop displacement of our reference models and models with different values of these three parameters. Each set includes three models with $\Delta L = -20$ km, 0 km and 20 km, and they all produce imbricate thrust, ramp-flat and duplex respectively. Small changes are visible in the process of faulting as well as in the final configuration of faults within the tested range of variations in these parameters, but the type of thrust geometry does not change. While inviting a more thorough investigation on the role of these parameters, these results justify our focus on the horizontal arrangement of the tips of décollements in the main text and support the main conclusion of this paper.

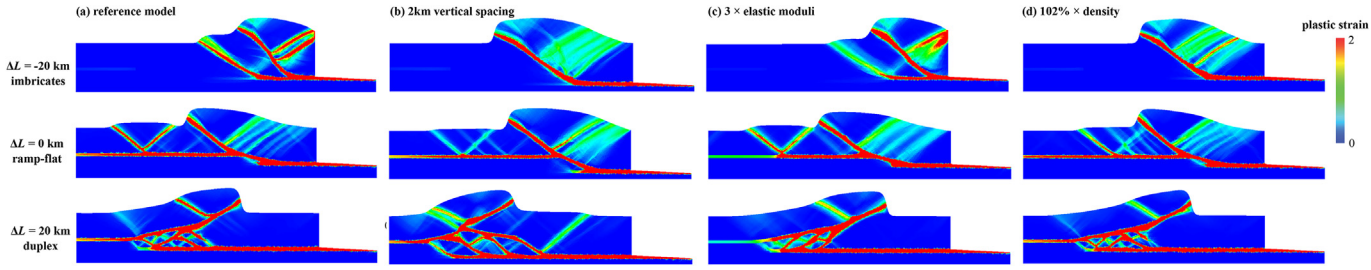

Fig. A1. Reference model (a) and extra models showing relatively low sensitivity of thrust geometry to (b) the vertical separation of weak layers, (c) elastic moduli (G and K) and (d) density (ρ).

A. 1 Sensitivity to the vertical separation of weak layers

Models discussed in the main text have a vertical separation between two weak layers of 1 km (Fig. A1a). We verified that increasing the vertical separation by a factor of 2 does not cause major changes in the correlation between the horizontal arrangement of décollements, represented by ΔL, and the resultant type of thrust geometry (Fig. A1b). Although there are some minor differences like the number of imbricate splays and internal deformation within a duplex, this set of models produced the same correspondence between thrust geometry and ΔL.

A. 2 Sensitivity to elastic moduli

Increasing the elastic moduli by a factor of 3 did not cause any significant change in the correspondence between the type of thrust geometry and ΔL (Fig. A1c).

A. 3 Sensitivity to density

Increasing density of strong layers from 2600 kg/m^3 to 2650 kg/m^3 and that of weak layers from 2500 kg/m^3 to 2550 kg/m^3 did not alter the correspondence between thrusting style and ΔL (Fig. A1d).

The tested amount of density change is only about 2% of the original density but a greater variation in density would weaken geological relevance.

References

Allen, P.A., 1997. Earth Surface Processes. Blackwell Sciences Ltd, Oxford, p. 404.

Apperson, K.D., Bartholomew, M.J., 1992. The effect of flat length on fault and footwall deformation. EOS Transac. Am. Geophys. Union 73 (43), 572.

Bartholomew, M.J., 1987. Structural evolution of the Pulaski thrust system, southwestern Virginia. Geol. Soc. Am. Bull. 99, 491–510.

Bartholomew, M.J., Brown, K.E., 1992. The Valley Coalfield (Mississippian age) in Montgomery and Pulaski Counties, Virginia with 1:100,000-scale Geologic Map of Devonian and Mississippian Rocks in Pulaski and Montgomery Counties, vol. 124. Virginia Division of Mineral Resources, Publication, p. 33.

Bartholomew, M.J., Lowry, W.D., 1979. Geology of the Blacksburg Quadrangle, Virginia, vol. 14. Virginia Division of Mineral Resources, Publication. G-81B (1:24,000-scale map with text).

Bartholomew, M.J., Whitaker, A.E., 2010. The Alleghanian deformational sequence at the foreland junction of the Central and Southern Appalachians. In: Tollo, R.P., Bartholomew, M.J., Hibbard, J.P., Karabinas, P.M. (Eds.), From Rodinia to Pangea: the Lithotectonic Record of the Appalachian Region, vol. 206. Geological Society of America Memoir, pp. 431–454.

Bartholomew, M.J., Milici, R.C., Schultz, A.P., 1980. Geologic Structure and Hydrocarbon Potential along the Saltville and Pulaski Thrusts in Southwestern Virginia and Northeastern Tennessee, vol. 23. Virginia Division of Mineral Resources, Publication (6 Sheets with text).

Bartholomew, M.J., Gathright, T.M., Henika, W.S., 1981. A tectonic model for the Blue Ridge in central Virginia. Am. J. Sci. 281, 1164–1183.

Bartholomew, M.J., Schultz, A.P., Henika, W.S., Gathright II, T.M., 1982. Geology of the Blue Ridge and Valley and Ridge at the junction of the central and southern Appalachians. In: Lyttle, P.T. (Ed.), Central Appalachian Geology, NE-SE GSA '82 Field Trip Guidebooks, vol. 266. American Geological Institute, pp. 121–170.

Bartholomew, M.J., Henika, W.S., Lewis, S.E., 1994. Geologic and structural transect of the New River Valley: Valley and Ridge and blue Ridge provinces, southwestern Virginia. In: Schultz, A.P., Henika, W.S. (Eds.), Field Guides to Southern Appalachian Stratigraphy, Structure, and Engineering Geology, Southeastern Section Meeting, Guidebook, vol. 10. Geological Society of America, Virginia Tech, pp. 177–228.

Belotti, H.J., Saccavino, L.L., Schachner, G.A., 1995. Structural styles and petroleum occurence in the Sub-Andean thrust belt of northern Argentina. In: Tankard, A.J., Suárez, S., Welsink, H.J. (Eds.), Petroleum Basins of South America, vol. 62. American Association of Petroleum Geologists Memoir, pp. 545–555.

Bonnet, C., Malavieille, J., Mosar, J., 2007. Interactions between tectonics, erosion, and sedimentation during the recent evolution of the Alpine orogen: analogue modelling insights. Tectonics 26, TC6016.

Boyer, S.E., Elliott, D., 1982. Thrust systems. Am. Assoc. Petrol. Geol. Bull. 66, 1196–1230.

Buck, W.R., 1988. Flexural rotation of normal faults. Tectonics 7 (5), 959–973.

Buiter, S.J.H., Babeyko, A.Y., Ellis, S., Gerya, T.V., Kaus, B.J.P., Kellner, A., Schreurs, G., Yamada, Y., 2006. The Numerical Sandbox: Comparison of Model Results for a Shortening and an Extension Experiment, vol. 253. Geological Society, London, Special Publication, pp. 29–64.

Choi, E., Tan, E., Lavier, L.L., Calo, V.M., 2013. DynEarthSol2D: an efficient unstructured finite element method to study long-term tectonic deformation. J. Geophys. Res. Solid Earth 118, 1–16.

Colmenares, L.B., Zoback, M.D., 2002. A statistical evaluation of rock failure criteria constrained by polyaxial test data for five different rocks. Int. J. Rock Mech. Min. Sci. 39, 695–729.

Couzens, B.A., Dunne, W.M., 1994. Displacement transfer at thrust terminations: the Saltville thrust and Sinking Creek anticline, Virginia, U.S.A. J. Struct. Geol. 16, 781–793.

Couzens, B.A., Dunne, W.M., Onasch, C.M., Glass, R., 1993. Strain variations and three-dimensional strain factorization at the transition from the Southern to the Central Appalachians. J. Struct. Geol. 15, 451–464.

Culling, W.E.H., 1960. Analytical theory of erosion. J. Geol. 68 (3), 336–344.

Cundall, P.A., Board, M., 1988. A microcomputer program for modeling large strain plasticity problems. In: Swoboda, G. (Ed.), Numerical Methods in Geomechanics, Processding of the 6th International Conference on Numerical Methods in Geomechanics, pp. 2101–2108.

Dahlen, F.A., Barr, T.D., 1989. Brittle frictional mountain building: 1. Deformation and mechanical energy budget. J. Geophys. Res. 94, 3906–3922.

Dahlstrom, C.D.A., 1970. Structural geology in the eastern margin of the Canadian Rocky Mountains. Bull. Can. Petrol. Geol. 18 (3), 332–406.

Davis, D., Suppe, J., Dahlen, F.A., 1983. Mechanics of fold-and-thrust belts and accretionary wedges. J. Geophys. Res. 88, 1153–1172.

Dean, S.L., Kulander, B.R., Skinner, J.M., 1988. Structural chronology of the Alleghanian orogeny in southeastern West Virginia. Geol. Soc. Am. Bull. 100, 299–310.

Dixon, J.S., 1982. Regional structural synthesis, Wyoming Salient of western overthrust belt. Am. Assoc. Petrol. Geol. Bull. 66 (10), 1560–1580.

Ellis, S., Schreurs, G., Panien, M., 2004. Comparisons between analogue and numerical models of thrust wedge development. J. Struct. Geol. 26, 1659–1675.

Engelder, T., Engelder, R., 1977. Fossil distortion and decollement tectonics on the Appalachian Plateau. Geology 5, 457–460.

Erickson, S.G., 1995. Mechanics of triangle zones and passive-roof duplexes: implications of finite element models. Tectonophysics 245, 1–11.

Evans, M.A., 1989. The structural geometry and evolution of foreland thrust systems, northern Virginia. Geol. Soc. Am. Bull. 101, 339–354.

Evans, M.A., 2010. Temporal and spatial changes in deformation conditions during the formation of the Central Appalachian fold-and-thrust belt: evidence from joints, vein mineral paragenesis, and fluid inclusions. In: Tollo, R.P., Bartholomew, M.J., Hibbard, J.P., Karabinas, P.M. (Eds.), From Rodinia to Pangea: the Lithotectonic Record of the Appalachian Region, vol. 206. Geological Society of America Memoir, pp. 477–552.

Gray, D.R., 1981. Compound tectonic fabrics in singly folded rocks from southwestern Virginia, U.S.A. Tectonophysics 78, 229–248.

Gwinn, V.E., 1964. Thin-skinned tectonics in the plateau and Northwestern Valley and Ridge provinces of the Central Appalachians. Geol. Soc. Am. Bull. 75, 863–900.

Gwinn, V.E., 1970. Kinematic patterns and estimates of lateral shortening, Valley and Ridge and Great Valley provinces, Central Appalachians, South-central Pennsylvania. In: Fischer, B.W., Pettijohn, F.J., Weaver, K.N. (Eds.), Studies of Appalachian Geology: Central and Southern. Wiley, New York, pp. 127–146.

Harris, L.D., Milici, R.C., 1977. Characteristics of thin-skinned style of deformation in the southern Appalachians, and potential hydrocarbon traps. U. S. Geol. Surv. Prof. Pap. 1018.

House, W.M., Gray, D.R., 1982. Displacement transfer at thrust terminations in Southern Applachians-saltville thrust as example. Am. Assoc. Petrol. Geol. Bull. 66 (7), 830–842.

Jaeger, J.C., Cook, N.G.W., 1976. Fundamentals of Rock Mechanics, second ed. Chapman and Hall, London, United Kingdom (GBR).

Konstantinovskaya, E., Malavieille, J., 2011. Thrust wedges with decollement levels and syntectonic erosion: a view from analog models. Tectonophysics 502 (3–4), 336–350.

Kühni, A., Pfiffner, O.A., 2001. Drainage patterns and tectonic forcing: a model study for the Swiss Alps. Basin Res. 13, 169–197.

Kulander, B.R., Dean, S.L., 1986. Structure and tectonics of central and southern Appalachian Valley and Ridge and Plateau Provinces, West Virginia and Virginia. Bull. Am. Assoc. Petrol. Geol. 70, 1674–1684.

Lavier, L.L., Buck, W.R., Poliakov, A.N.B., 2000. Factors controlling normal fault offset in an ideal brittle layer. J. Geophys. Res. 105 (B10), 23,431–23,442.

Malavieille, J., 2010. Impact of erosion, sedimentation, and structural heritage on the structure and kinematics of orogenic wedges: analog models and case studies. GSA Today 20, 4–10.

Mitra, S., 1986. Duplex structures and imbricate thrust systems: geometry, structural position, and hydrocarbon potential. Am. Assoc. Petrol.Geol. Bull. 70, 1087–1112.

Mitra, S., 1988. Three-dimensional geometry and kinematic evolution of the Pine Mountain thrust system, southern Appalachians. Geol. Soc. Am. Bull. 100, 72–95.

Nickelsen, R.P., 1988. Structural evolution of folded thrusts and duplexes on a first-order anticlinorium in the Valley and Ridge Province of Pennsylvania. In: Mitra, G., Wojtal, S. (Eds.), Geometries and Mechanisms of Thrusting, with Special Reference to the Appalachians, vol. 222. Geological Society of America Special Paper, pp. 89–106.

Onasch, C.M., Dunne, W.M., 1993. Variation in quartz arenite deformation mechanisms between a roof sequence and duplexes. J. Struct. Geol. 15, 465–475.

Panian, J., Wiltschko, D., 2004. Ramp initiation in a thrust wedge. Nature 427, 624–627.

Poliakov, A.N.B., Herrmann, H.J., Podladchikov, Y.Y., Roux, S., 1994. Fractal plastic shear bands. Fractals 2, 567–581.

Price, R.A., 1981. The Cordilleran foreland thrust and fold belt in the southern Canadian Rocky Mountains. In: McClay, K.R., Price, N.J. (Eds.), Thrust and Nappe Tectonics, vol. 9. Geological Society, London, Special Publication, pp. 427–448.

Price, R.A., Fermor, P.R., 1985. Structure Section of the Cordilleran Foreland Thrust and Fold Belt West of Calgary, Alberta. Geological Survey of Canada Paper, pp. 14–84.

Ramsay, J.G., 1981. Tectonics of the Helvetic Nappes, vol. 9. Geological Society, London, Special Publication, pp. 293–309.

Rich, J.L., 1934. Mechanics of low-angle overthrust faulting as illustrated by cumberland thrust block, Virginia, Kentucky and Tennessee. Am. Assoc. Petrol. Geol. Bull. 18, 1584–1596.

Rodger, J., 1950. Mechanics of Appalachian folding as illustrated by sequatchie anticline, Tennessee and Alabama. Bull. Am. Assoc. Petrol. Geol. 34 (4), 672–681.

Ruh, J.B., Kaus, B.J.P., Burg, J.-P., 2012. Numerical investigation of deformation mechanics in fold-and-thrust belts: influence of rheology of single and multiple décollements. Tectonics 31, TC3005.

Schultz, A.P., 1979. Field trip guide—Second day. In: Lowry, W.D. (Ed.), Nature of Thrusting along the Allegheny Front Near Pearisburg and of Overthrusting in the Blacksburg-Radford Area of Virginia, vol. 8. Virginia Polytechnic Institute and State University Department of Geological Sciences Guidebook, pp. 55–66.

Schultz, A.P., 1986. Broken formations of the Pulaski thrust sheet near Pulaski, Virginia. In: McDowell, R.C., Glover III, L. (Eds.), The Lowry Volume: Studies in Appalachian Geology, vol. 3. Virginia Polytechnic Institute and State University Department of Geological Sciences Memoir, pp. 13–26.

Schultz, A.P., 1988. Horses in fensters of the Pulaski thrust sheet, southwestern Virginia: structure, kinematics, and implications for hydrocarbon potential of the eastern overthrust belt. U. S. Geol. Surv. Bull. 1839A, A1–A13.
Schultz, A.P., Bartholomew, M.J., 2009. Geologic Map of the Staffordsville Quadrangle, Virginia. Virginia Division of Geology and Mineral Resources. Open File Report 09-02, 1:24,000–scale map.
Schultz, A.P., Bartholomew, M.J., 2010. Geologic Map of the Radford South Quadrangle, Virginia. Virginia Division of Geology and Mineral Resources. Open File Report 10-8, 1:24,000–scale map.
Sears, J.W., Schmidt, C.J., Dresser, H.W., Hendrix, T., 1989. A geological transect from the Highland Mountains foreland block through the southwest Montana thrust belt to the pioneer batholith. In: Sears, J.W. (Ed.), Tobacco Root Geological Society 14th Annual Field Conference "Structure, Stratigraphy and Economic Geolgoy of the Dillon Area", Northwest Geolgoy, vol. 18, pp. 1–20.
Selzer, C., Buiter, S.J.H., Pfiffner, O.A., 2007. Sensitivity of shear zones in orogenic wedges to surface processes and strain softening. Tectonophysics 437 (1–4), 51–70.
Simon, R.I., Gray, D.R., 1982. Interrelations of mesoscopic structures and strain across a small regional fold, Virginia Appalachians. J. Struct. Geol. 4, 271–289.
Simpson, G., 2009. Mechanical modelling of folding versus faulting in brittle–ductile wedges. J. Struct. Geol. 31, 369–381.
Simpson, G., 2011. Mechanics of non-critical fold–thrust belts based on finite element models. Tectonophysics 499, 142–155.
Smart, K.J., Couzens-Schultz, B.A., 2001. Mechanics of blind foreland thrusting: comparison of numerical and physical modeling. J. Geol. 109, 771–779.
Smart, K.J., Dunne, W.M., Krieg, R.D., 1997. Roof sequence response to emplacement of the Wills Mountain blind duplex: the roles of forethrusting and scales of deformation. J. Struct. Geol. 19, 1443–1459.
Smart, K.J., Krieg, R.D., Dunne, W.M., 1999. Deformation behavior during blind thrust translation as a function of fault strength. J. Struct. Geol. 21, 855–874.
Spraggins, S.A., Dunne, W.M., 2002. Deformation history of a forleand thrust belt in a recess: an example from the Roanoke recess, Appalachains, USA. J. Struct. Geol. 24, 411–433.
Stanley, R.S., Ratcliffe, N.M., 1985. Tectonic synthesis of the Taconian orogeny in western New England. Geol. Soc. Am. Bull. 96, 1227–1250.
Stockmal, G.S., Beaumont, C., Nguyen, M., Lee, B., 2007. Mechanics of thin-skinned fold-and-thrust belts: insights from numerical models. Geol. Soc. Am. Special Pap. 433, 63–98.
Suppe, J., 1980. Imbricated structure of western foothills belt, southcentral Taiwan. Petrol. Geol. Taiwan 17, 1–16.
Vardoulakis, I., 1980. Shear band inclination and shear modulus of sand in biaxial tests. Int. J. Numer. Anal. Methods Geomech. 4, 103–119.
Whitaker, A.E., Bartholomew, M.J., 1999. Layer parallel shortening: a mechanism for determining deformation timing at the junction of the central and southern Appalachians. Am. J. Sci. 299 (3), 238–254.
Williams, W.D., Dixon, J.S., 1985. Seismic interpretation of the Wyoming overthrust belt. In: Gries, R.R., Dyer, R.C. (Eds.), Seismic Exploration of Rocky Mountain Region. Rocky Mountain Association of Geology, Denver, Colorado, pp. 13–22.
Wilson, T.H., 1989. Geophysical studies of large blind thrust, Valley and Ridge Province, Central Appalachians. Am. Assoc. Petrol. Geol. Bull. 73 (3), 276–288.
Wilson, T.H., Shumaker, R.C., 1992. Broad Top thrust sheet: an extensive blind thrust in the central Appalachians. Bull. Am. Assoc. Petrol. Geol. 76, 1310–1324.
Wojtal, S., 1992. Shortening and elongation of thrust zones within the Appalachian foreland fold-thrust belt. In: Mitra, S., Fisher, G.W. (Eds.), Structural Geology of Fold and Thrust Belts. The Johns Hopkins University Press, Baltimore, MD, pp. 93–103.
Zoback, M.D., 2007. Reservoir Geomechanics. Cambridge University Press, New York.